Heat-induced bubble expansion as a route to increase the porosity of foam templated bio-based macroporous polymers

Wenzhe Song[a], Kevin Barber[b], Koon-Yang Lee[a,*]

[a]The Composites Centre, Department of Aeronautics, Imperial College London, South Kensington Campus, London, SW7 2AZ, UK

[b]Thermo Fisher Scientific, Hemel Hempstead, HP2 7GE, UK

*Corresponding author. Tel.: +44 (0)20 7594 5150; E-mail: koonyang.lee@imperial.ac.uk

Abstract

Macroporous polymers were prepared by mechanically frothing a bio-based epoxy resin and hardener mixture to first create air-in-resin liquid foam, followed by curing of the liquid foam. It was found that heating the air-in-resin liquid foam prior to its gelation decreased the viscosity of the resin mixture and increased the pressure of the air bubbles, leading to an isotropic expansion of the air bubbles. This resulted in an increase in porosity of the resulting macroporous polymers from 71% to 85%. Correspondingly, the compressive modulus (E) and strength (σ) of the macroporous polymers decreased from 231 MPa and 5.9 MPa, respectively, to 58 MPs and 1.9 MPa, respectively. This decrease is attributed to an increase in porosity and pore throat frequency of the foam-templated macroporous polymers when heat was applied to the liquid foams. The deformation of the pores based on in situ SEM micro-compression test of the fabricated macroporous polymers is also discussed.

Keywords

Macroporous polymer, mechanical frothing, compression properties

1.0 Introduction

Polymer foams or macroporous polymers are lightweight materials of great commercial importance, with an estimated global market value of US$172 billion by 2021 [1]. They are often used in industries where weight saving is critical, such as the construction [2],

packaging [3] and the automotive industries [4]. The most commonly used polymer foams are made from polyurethane, polystyrene or poly(vinyl chloride). They represent ~90 % of the market share for polymeric foams in 2015 [5]. However, heavy environmental legislations and public's growing demand for greener materials have sparked the development of environmental friendlier materials. Therefore, extensive research efforts have been poured into the development of bio-based or bio-derived polymer foams. Polymer foams derived from starch [6-8], poly(3-hydroxybutyrate-co-3-hydroxyvalerate) [9, 10], polylactide [11-13], polycaprolactone [14], bio-derived polyurethane [15, 16] and bio-based epoxy resins [17, 18] have been produced and studied. Among these, bio-based epoxy foams have attracted significant attention due to their good thermal stability compared to other bio-based thermoplastics [19], high chemical and moisture resistance [20], as well as high specific mechanical properties [21].

Numerous methods can be used to produce (bio-based and non bio-based) epoxy foams. Syntactic epoxy foams can be produced by dispersing hollow microspheres, typically made from glass [22] or phenolics [23], into the liquid epoxy resin, followed by curing of this resin. The porosity of syntactic foams is controlled by the concentration of hollow microspheres in the resin. While it is desirable to increase the concentration of hollow microspheres to increase the porosity of syntactic foams, excessive microspheres will result in a dramatic increase in the viscosity of the resin-microspheres dispersion, leading to processing difficulties [24]. Epoxy resin can also be foamed during its curing process with the use of physical or chemical blowing agents. Physical blowing agents are mainly low boiling points hydrocarbons, such as pentane, toluene and hexane [25]. They are added into the epoxy resin as liquid at room temperature and vaporised upon heating during the curing of the resin to produce cellular structures. Chemical blowing agents, on the other hand, generate gaseous products via chemical reactions upon heating. Ammonium carbonate [26],

azodicarbonamide [27] and sodium borohydride [28] are used as chemical blowing agents to produce epoxy foams. Ammonium carbonate decomposes into ammonia, carbon dioxide and water when heated. Azodicarbonamide produces ammonia, nitrogen and isocyanic acid upon heating, and sodium borohydride reacts with water to generate hydrogen and sodium metaborate.

We have recently developed a blowing agent- and stabiliser-free, foam-templating method to produce macroporous polymers derived from bio-based epoxy resin [29]. This was achieved by first creating an air-in-epoxy resin liquid foam using mechanical frothing, followed by curing of this liquid foam at room temperature to produce the bio-based macroporous polymers. The compressive modulus and strength of these macroporous polymers were found to be 163 MPa and 4.9 MPa, respectively. While this manufacturing route is green, simple and versatile, the density of these macroporous polymers is limited to ~0.29 g cm^{-3}. In order to widen the applications of these foam-templated bio-based macroporous polymers, it is desirable to further reduce the density of these mechanically-frothed bio-based epoxy foams. Therefore in this work, we build upon our previous work [29, 30] and present a simple method to increase the porosity of foam-templated bio-based macroporous polymers based on air bubble expansion. By using heat, the air bubbles trapped within the air-in-epoxy resin liquid foams can be expanded, thereby increasing the porosity of the resulting foam-templated bio-based macroporous polymers. The morphology and mechanical properties of these bio-based macroporous polymers are characterised and the influence of the pore structures on the measured compression properties of the macroporous polymers is also discussed.

2.0 Experimental

2.1 Materials

A high biomass content epoxy resin (Greenpoxy 56, biomass carbon percentage = 56 ± 2 %, ρ = 1.20 ± 0.01 g cm^{-3}, η = 2500 mPa s at 15 °C) and an amine-based hardener (GP 505, biomass carbon percentage = 58 ± 3 %, ρ = 0.99 ± 0.01 g cm^{-3}, η = 2600 mPa s at 15 °C) were purchased from Matrix Composite Materials Company Ltd (Bristol, UK) and used as the bio-based epoxy resin for the preparation of foam-templated macroporous polymers.

2.2 Heat-induced bubble expansion of foam-templated bio-based macroporous polymers

Foam-templated bio-based macroporous polymers were prepared by mechanical frothing a mixture of epoxy resin and hardener following previously described methods [29, 30]. Briefly, 75 g of bio-based epoxy resin and 30 g of amine-based hardener were poured into a Pyrex glass bowl and this mixture was mechanically frothed using a hand-held mixer (HM730B, Sainsbury's, London, UK) operated at maximum power output of 200 W for 20 min to produce an air-in-resin liquid foam. The liquid foam was then poured into self-standing Falcon® tubes (25 mm in diameter and 115 mm in height) and left to cure at room temperature for 24 h, followed by a post-curing step at 40 °C for another 24 h (sample **0**). To increase the porosity of the foam-templated bio-based macroporous polymers, the prepared air-in-resin liquid foam was left at room temperature for only 40 min (**1**) and 10 min (**2**), respectively, followed by a curing step at elevated temperatures of 80 °C (**A**), 100 °C (**B**) and 120 °C (**C**), for 24 h in an oven pre-heated to the desired curing temperatures. The samples left at room temperature for 40 min (samples **1**) and 10 min (samples **2**) correspond to 1 h (20 min of mechanical frothing, followed by 40 min of standing time at room temperature) and 30 min (20 min of mechanical frothing, followed by 10 min of standing time at room temperature) after the initial mixing of the bio-based epoxy resin and hardener.

2.3 Preparation of bulk polymers cured at different conditions

As the macroporous polymers were fabricated by curing the air-in-resin liquid foams at different time after initial mixing and temperatures, the changes in curing temperatures could affect the mechanical performance of the resulting pore wall materials (struts) and hence, the overall mechanical performance of the resulting bio-based macroporous polymers. Therefore, bulk polymers without air bubbles were also prepared and tested. 75 g of bio-based epoxy resin and 30 g of hardener were mixed for 10 min in a paper cup using a wooden stick. The stirring of the mixture was kept slow and gentle to avoid trapping any air bubbles in the resin-hardener mixture. To prepare compression test specimens, the well-mixed resin-hardener mixture was poured into Falcon® tubes with diameter and height of 15 mm and 115 mm, respectively. Tensile test specimens were prepared by pouring the well-mixed resin-hardener mixture into silicon rubber-based dumbbell shaped moulds, whereby the dumbbells possessed an overall length and thickness of 75 mm and 1.5 mm, respectively. The narrowest part of the dumbbells was 5 mm. To fabricate flexural test specimens, the resin-hardener mixture was poured into a 240 × 80 × 5 mm^3 metal mould coated with PTFE release agent. All the samples were cured following the conditions previously described.

2.4 Characterisation of the foam-templated bio-based macroporous polymers

2.4.1 Structure and morphology of the macroporous polymers

The internal structure of the foam-templated bio-based macroporous polymers was investigated using scanning electron microscope (SEM) (Hitachi S-3700N, Tokyo, Japan) operating at an accelerating voltage of 15 kV. Prior to SEM, the macroporous polymers were cut into cylinders (diameter = 25 mm and height = 5 mm) and broken into two halves by hand to reveal the internal structure of the macroporous polymers. The samples were then mounted onto aluminium stubs using carbon tabs, followed by Au coating (Agar Auto Sputter Coater, Essex, UK) at 40 mA for 1 min. The average pore diameter (D_{pore}), average pore throat

diameter[1] (D_{throat}) and pore throat frequency[2] (f_{throat}) were determined from these SEM images with a population size of 600 pores. The mean pore wall thickness (t_{wall}) was calculated using the Aleksandrov's equation [31]:

$$t_{wall} = D_{pore}\left(\frac{1}{\sqrt{1-\rho_f/\rho_s}} - 1\right) \quad (1)$$

where ρ_{f} and ρ_{s} are the foam density of the macroporous polymers and the true density of the solid polymers (see section 2.4.2).

2.4.2 Density, porosity and open cell content of the macroporous polymers

Prior to determining the foam density of the macroporous polymers (ρ_{f}), the prepared samples were lathed and cut to produce cylindrical samples with uniform diameter (d) and height (h). ρ_{f} was then calculated from the measured d, h and the mass (m) of the cylindrical samples using the equation:

$$\rho_{\text{f}} = \frac{4m}{\pi d^2 h} \quad (2)$$

The true density of the solid polymers (ρ_{s}) was determined from the bulk polymers without air bubbles using He pycnometry (Accupyc II 1340, Micromeritics Ltd, Hexton, UK). The porosity (P) of the macroporous polymers was calculated using:

$$P = \left(1 - \frac{\rho_{\text{f}}}{\rho_{\text{s}}}\right) \times 100\% \quad (3)$$

The open cell content (O_V) of the macroporous polymers was determined in accordance to ASTM D6226–15. Rectangular macroporous polymer test specimens with dimensions of $12 \times 12 \times 25$ mm^3 were prepared and their open porous skeletal density (ρ_{skel}) were determined using He pycnometer. The open cell content of the macroporous polymers was calculated using:

$$O_V = \left(1 - \frac{\rho_{\text{f}}}{\rho_{\text{skel}}}\right) \times 100\% \quad (4)$$

1 $D_{\text{throat}} = \frac{1}{n}\sum_{i=1}^{n} D_{\text{throat},\,i}$ where $D_{\text{throat},\,i}$ and n correspond to the diameter of the pore throat i and the number of pore throats observed within our pore population size of 600 pores, respectively.

2 $f_{\text{throat}} = \frac{p}{600}$ where p is the number of pore throats observed within our pore population size of 600.

2.4.3 Compressive properties of the foam-templated macroporous polymers

The compressive properties of the macroporous polymers were determined in accordance to ASTM D1621–10 using an Instron universal tester (Model 5969, Norwood, USA) equipped with a 50 kN load cell. Cylindrical compression test specimens with both diameter and height of 24 mm were placed between two flat and parallel polished plates prior to loading the test specimens at a crosshead displacement speed of 1 mm min^{-1}. A total of five specimens were tested for each sample at room temperature. The compliance of the compression test equipment was found to be 1.8×10^{-5} mm N^{-1}.

2.4.4 In-situ SEM micro-compression test of the bio-based macroporous polymers

In-situ SEM micro-compression test was performed using a micro-compression tester (Deben Microtest Stage, Suffolk, UK) equipped with a 5 kN load cell placed in an SEM chamber (Hitachi S-3700N, Tokyo, Japan). Prior to the test, cubic specimens of the macroporous polymers with dimensions of $10 \times 10 \times 10$ mm^3 were cut and coated with Au (Agar Auto Sputter Coater, Essex, UK) at 40 mA for 1 min. The test specimens were then compressed at a crosshead displacement speed of 0.5 mm min^{-1} and the morphology of the compressed cubic test specimens were imaged every 30 s.

2.5 Characterisation of the resin-hardener mixture and the bulk polymers cured at different conditions

2.5.1 Viscosity of the resin-hardener mixture

The rheology of the resin-hardener mixture as a function of temperature and time after initial mixing was determined using a rotational rheometer (HAAKE MARS 60, Thermo Fisher Scientific, Hemel Hempstead, UK) equipped with a plate-plate (35 mm diameter) geometry. Prior to the test, the resin and hardener were mixed gently in a paper cup to avoid trapping any air bubbles. The mixed resin-hardener mixture was then placed between two parallel disposable aluminium plates and the gap between the plates was set to be 1 mm. Rheological

characterisation for the various curing conditions used in this work were conducted in oscillatory mode at frequency and strain of 1 Hz and 0.5 %, respectively.

2.5.2 Compressive properties of the bulk polymers

The compressive properties of the bulk polymers were determined in accordance to ASTM D695–15 using an Instron universal tester (Model 5969, Norwood, USA). The load cell and crosshead displacement speed used were 50 kN and 1 mm min^{-1}, respectively. Prior to the test, the previously prepared cylindrical bulk polymer specimens (see section 2.3) were lathed and cut into cylinders with diameter and height of 12 mm and 24 mm, respectively. The test specimens were loaded in compression between two flat and parallel polished plates. A video extensometer (Imetrum Video Gauge, Bristol, UK) was used to monitor the strain of the test specimens. A total of five specimens were tested at room temperature for each sample.

2.5.3 Tensile properties of the bulk polymers

The tensile properties of the bulk polymers were determined in accordance to ASTM D638–14 using an Instron universal tester (Model 5969, Norwood, USA) equipped with a 1 kN load cell. The dumbbell-shaped test specimens (section 2.3) possessed a gauge length of 25 mm. A total of five specimens were tested at room temperature for each sample at a crosshead displacement speed of 1 mm min^{-1}. The strain of the test specimens was monitored using a video extensometer (Imetrum Video Gauge, Bristol, UK).

2.5.4 Flexural properties of the bulk polymers

The flexural properties of the bulk polymers were determined in accordance to ASTM D790–15 using an Instron universal tester (Model 5969, Norwood, USA) equipped with a 1 kN load cell at room temperature. Prior to the test, the previously prepared bulk polymers (section 2.3) were cut into rectangular specimens with dimensions of 100 × 90 × 5 mm^3. The span length used was 80 mm and the test specimens were loaded in 3-point bending mode at a crosshead displacement speed of 2 mm min^{-1}.

2.5.5 Molecular weight between crosslinks of the bulk polymers

The average molecular weight between crosslinks (M_c) of the bulk polymers polymerised at different conditions was estimated from the glass transition temperature (T_g) and the storage modulus of the rubbery plateau (E'_R) using the following equation [32]:

$$M_c = \frac{3\varphi\rho_s R(T_g+40)}{E'_R} \quad (5)$$

where φ is the mean-square end-to-end chain distance in the polymer network over the chain distance in free space, which was found to be very close to 1 for cured epoxy resin [33]. R, T_g and E'_R are the universal gas constant (8.31 J mol^{-1} K^{-1}), the glass transition temperature (based on the temperature at the peak of the tan δ curve) [34] and the storage modulus of the rubbery plateau evaluated at T_g + 40 K, respectively. The viscoelastic properties of the bulk polymers were determined using dynamic mechanical thermal analysis (DMTA) (RSA-G2, TA Instruments, New Castle, UK) conducted on test specimens with dimensions of 30 × 5 × 1.5 mm^3 in 3-point bending mode (span = 25 mm). The test specimens were heated from 25 °C to 150 °C at a rate of 5 °C min^{-1}. The frequency and strain amplitude used were 1 Hz and 0.005%, respectively.

3.0 Results and discussion

3.1 Density, porosity, and morphology of the macroporous polymers

The SEM images of the foam-templated bio-based macroporous polymers cured at various conditions are shown in fig 1 and the foam density (ρ_f), porosity (P), open cell content (O_V), average pore diameter (D_{pore}), mean pore wall thickness (t_{wall}), average pore throat diameter (D_{throat}) and pore throat frequency (f_{throat}) of the fabricated bio-based macroporous polymers are summarised in table 1. Spherical pores can be observed for all samples. This is consistent with our previous study [29]. The formation of spherical pores is a direct result of the trapped air bubbles reaching equilibrium with the surrounding resin prior to gelation as spherical shape minimises surface tension.

Air-in-resin liquid foam cured at room temperature for 24 h followed by post curing at 40 °C for another 24 h (sample **0**) possessed a porosity of 71 % and D_{pore} of 152 μm (table 1). By reducing the time after initial mixing of the air-in-resin liquid foam at room temperature to only 1 h before curing at elevated temperatures of 80 °C (sample **1-A**), 100 °C (sample **1-B**) and 120 °C (sample **1-C**), respectively, the porosity of the resulting bio-based macroporous polymers increased up to 78 %. This is accompanied by an increase in D_{pore} of the macroporous polymers from 152 μm for sample **0** to 187 μm for sample **1-C**. A further reduction in the time after initial mixing of the air-in-resin liquid foam to only 30 min before curing at elevated temperatures of 80 °C (sample **2-A**), 100 °C (sample **2-B**) and 120 °C (sample **2-C**) increased the porosity of the resulting macroporous polymers further up to 85%, with a D_{pore} of 352 μm (sample **2-C**). These results can be attributed to the air-in-resin liquid foams 30 min and 1 h after initial mixing not reaching their gelation point prior to heating, as well as the increase in pressure inside the air bubbles of the liquid foams upon heating. This leads to the expansion of the air bubbles trapped in the air-in-resin liquid foam, producing macroporous polymers with higher porosity and larger D_{pore}.

In addition to this, the viscosity of the resin also decreased upon heating of the air-in-resin liquid foam prior to gelation (see fig 2). The viscosity of the resin-hardener mixture left to cure at room temperature (fig 2a, correspond to sample **0**) increased exponentially after initial mixing. This increase is consistent with the viscosity of epoxy resin systems as a function of time reported in the literature [35-37]. The viscosity of resin-hardener mixtures dropped sharply upon heating initially (figs 2b-d and 2e-g for 1 h and 30 min after initial mixing of the resin-hardener mixture, corresponding to samples **1-A** to **1-C** and **2-A** to **2-C**, respectively), followed by vitrification of the resin (a sharp increase in viscosity). The initial decrease in viscosity further aided the expansion of the air bubbles at elevated temperatures. Phase separation of liquid foams could potentially occur upon heating as the viscosity of the

liquid decreases, leading to air bubble coalescence. Nevertheless, this was not observed in our study due to the short time (less than 8 min) between viscosity decrease upon heating and the vitrification of the resin system. This prevented the complete phase separation of the air-in-resin liquid foam prior to resin vitrification.

Pore throats can also be observed on all samples. A pre-requisite for pore throat formation is the rupture of the thin pore walls between two adjacent pores [38, 39]. The formation of pore throats in foam-templated macroporous polymers can also be attributed to the incomplete coalescence of two air bubbles during curing [29]. Sample **0** possessed a pore throat diameter and pore throat frequency of 18 μm and 4%, respectively. By reducing the time after initial mixing to 1 h followed by curing at elevated temperatures, the pore throat diameter and pore throat frequency increased to 23 μm and 13 % (sample **1-A**), 31 μm and 17 % (sample **1-B**) and 36 μm and 20 % (sample **1-C**), respectively. The open cell content also increased from 2% (sample 0) to ~20% (samples 1). This is due to the expansion of air bubbles at elevated temperatures, causing the adjacent bubbles to touch and coalescence. As the viscosity of the resin decreased only for a short period of time before resin vitrification occurred, the coalescence of the air bubbles was incomplete, leading to the formation of pore throats and an increase pore throat frequency, as well as an increase in the open cell content of the macroporous polymers. Comparing samples **1** and **2**, D_{throat}, f_{throat} and O_V of samples **2-A**, **2-B** and **2-C** increased compared to samples **1-A**, **1-B**, **1-C** and **0**, as the resin viscosity of samples **2** upon heating was lower (due to shorter time after initial mixing) than samples **1** and **0**. It should be noted that the macroporous polymers fabricated were not air permeable as the pores observed were only partially interconnected.

3.2 Compression properties of the macroporous polymers

The representative compression stress-strain curves of the foam-templated bio-based macroporous polymers are shown in fig 3. All the curves possess three characteristic regions:

(i) a linear elastic region of up to ~5 % strain, (ii) a plateau region where the stress remained almost constant with increasing strain and (iii) a densification region where the compressive stress increased rapidly again. In the linear elastic region, the macroporous polymers deformed reversibly via pore wall bending [40]. When the force applied on the pore walls (struts) exceeded the plastic moment, the macroporous polymer yielded [41, 42]. At this point, the pore walls (struts) were bent plastically and the deformation of the macroporous polymers was no longer recoverable upon removal of the applied stress. After yielding, the compressive stress of the macroporous polymers stayed constant with increasing strain. This indicates that the presence of air trapped in the pores has little or no effect on the compressive properties of these macroporous polymers [40]. In the densification region of the stress-strain curves, most of the pores were completely crushed and the porous polymers behave like bulk polymers, causing the steep increase of stress with increasing strain. The compressive properties of the macroporous polymers cured at different conditions are summarised in table 2. Sample **0** possessed compressive modulus and strength of 231 MPa and 5.9 MPa, respectively. By reducing the time after initial mixing to 1 h before curing at elevated temperatures, the compressive properties of the resulting macroporous polymers decreased to E = 125 MPa and σ = 3.8 MPa (sample **1-C**). A further reduction of the time after initial mixing to only 30 min before curing at elevated temperatures further reduced the compressive properties of the macroporous polymers to E = 58 MPa and σ = 1.9 MPa (sample **2-C**).

To ascertain whether the changes in the curing conditions of the air-in-resin liquid foam affected the compressive properties of the bio-based macroporous polymers, we further investigated the degree of crosslinking of the bulk polymers cured at the same conditions as the macroporous polymers. The average molecular weight between crosslinks (M_c) of the bulk polymers were estimated from the viscoelastic properties (see fig 4) using equation 4.

M_c reduced with increasing polymerisation temperature (see table 3). This is also accompanied by an increase of the T_g of sample **0** from ~65 °C to ~91 °C for the rest samples. This is due to the formation of more crosslinks when the curing temperature was increased and a higher degree of crosslinking results in a higher glass transition temperature and a lower value of M_c. Nevertheless, the difference in M_c was not significant amongst all samples. This is also consistent with the mechanical properties of these bulk polymers (see table 4). Sample **0** possessed compressive modulus and strength of E = 3.2 GPa and σ = 82 MPa, tensile modulus and strength of E = 2.6 GPa and σ = 52 MPa and flexural modulus and strength of E = 2.5 GPa and σ = 70 MPa, respectively. By curing the bulk polymers at various conditions studied in this work, no significant differences in the mechanical properties of the bulk polymers can be observed. This further implies that the mechanical properties of the pore wall materials (struts) of our fabricated macroporous polymers are also similar to each other.

3.3 In-situ SEM micro-compression test of the macroporous polymers

The mechanical properties of porous materials are also influenced by their pore structures [43-47]. Therefore, in-situ SEM micro-compression test was carried out to investigate the micro-deformation process of the fabricated macroporous polymers. Exemplarily fracture process of samples **0** and **2-C** are shown in figs 5a and 5b, respectively. The videos of the in-situ SEM micro-compression test of all samples can be found in supporting information. When the strain of the test specimens was low, both samples deformed elastically and no visible cracks can be seen (figs 5a-1 and 5b-1). As the strain increased, small cracks can be observed in figs 5a-2 and 5b-2 (see arrows). Corrugations on the pore walls of sample **2-**C can also be seen. A further increase in strain of the samples led to the propagation and joining of cracks, forming localised crack lines (figs 5a-3 and 5b-3). The previously observed corrugation in sample **2-C** fractured. At this point, both samples started to yield due to the

irreversible displacement along the localised crack lines. The propagation of the cracks continued and the localised crack lines joined together throughout the samples (Figs 5a-4 and 5b-4). Beyond this specimen strain, the pores along the crack lines were crushed and these crack lines became crush bands. These bands are generally perpendicular to the compression direction [48, 49].

3.4 Discussion: The effect of different curing conditions on the compression properties of foam-templated bio-based macroporous polymers

Different curing conditions of the initial air-in-epoxy resin liquid foams led to the fabrication of macroporous polymers with different foam densities, pore throat frequencies and pore diameters. Ashby-Gibson model showed that the compression properties of macroporous polymers are dependent only on the relative density, $\frac{\rho_f}{\rho_s}$, of the macroporous polymers. Table 5 summarises the normalised compressive properties of the foam templated macroporous polymers studied in this work. The compressive moduli and strength of the macroporous polymers are normalised against ρ_f^2 and $\rho_f^{1.5}$, respectively [40]. It can be seen from this table that the normalised compressive properties of the macroporous polymers are similar for all samples. As no significant difference was observed in the mechanical properties of the pore wall materials (struts), the reduction in the compression properties of the fabricated macroporous polymers in this work can be mainly attributed to the reduction in the density of the macroporous polymers. In addition to this, pore throats can also be regarded as flaws on the pore walls and cracks can easily form and propagate from the pore throats. Many of the cracks observed in sample **2-C** (fig 5b) were initiated from pore throats and the crack line passed through these pore throats. Since the pore throat frequency increased with increasing the porosity of the macroporous polymers, the presence of pore throats further reduced the compression properties of the macroporous polymers observed in this study.

We also investigated the pore deformation of our fabricated macroporous polymers. Fig 6 shows the degree of pore deformation, defined as the ratio between the horizontal and vertical Feret diameters of the pores, $\frac{F_{\mathrm{h}}}{F_{\mathrm{v}}}$, for 2 different pore sizes of all samples. A $\frac{F_{\mathrm{h}}}{F_{\mathrm{v}}}$ value of unity and zero correspond to perfect spheres (as-fabricated pore) and a line (fully crushed pore), respectively. At any given specimen strain, it can be seen from this figure that larger pore deformed more compared to smaller pores. Several pore deformation mechanisms have been proposed, including cell rib bending, pore wall buckling, stretching and bending [50, 51]. Considering the relatively high foam density (~0.3 g cm^{-3}) of our macroporous polymers, the bending of the pore wall is the dominant pore deformation mechanism [52]. It can be anticipated that the deflection of the pore wall materials (struts) at a given load will be larger for larger pores. This implies that macroporous polymers with larger D_{pore} will deform easier than macroporous polymers with smaller D_{pore}. This is consistent with our observations that the compressive modulus and yield strength of the macroporous polymers decreased with increasing D_{pore}. Similar observations were also observed by other researchers [53, 54], whereby the fracture of a macroporous polymer initiates from pores of larger diameter.

3.5 Heat-induced bubble expansion of our liquid epoxy foam and commercially available thermoplastic foams: Similarities and differences

Our heat-induced bubble expansion of foam-templated macroporous polymers is analogous to the production of commercially available Zotefoams [55]. Zotefoams are crosslinked polyethylene (PE) foams produced by first saturating PE melt with nitrogen gas at high pressure (~700 bar in an autoclave). The pressure is then rapidly reduced to atmospheric pressure, supersaturating the PE melt and this allows for the nucleation of nitrogen gas bubbles within the polymer melt. This is then followed by a fast quenching step to room temperature to entrap the nitrogen gas bubbles within the solid PE, forming a “semi-foam” with porosity of approximately 30%. The “semi-foam” is then re-heated to temperatures close

to the melting point of PE under moderate pressure to expand the nitrogen gas bubbles, progressively releasing the entrapped nitrogen gas, producing the final low density closed-cell foam.

While both the Zotefoams process and the process reported in our work explore the use of heat to increase the porosity of macroporous polymers, it should be noted that the manufacturing process of Zotefoams require the use of autoclaves to saturate the PE melt with nitrogen gas at high pressure. In our macroporous polymer manufacturing method, air is dispersed directly into the liquid resin by high intensity mixing. The macroporous polymers in our work was found to possess more pore throats and more open-cell structure (see section 3.1) compared to the closed-cell Zotefoams. This can be attributed to both the volume occupied by nitrogen/air bubbles at the point of bubble expansion. As aforementioned, the "semi-foam" of Zotefoams possessed a porosity of approximately 30%. This implies that the nitrogen bubbles in the "semi-foam" have more space between adjacent nitrogen bubbles to expand prior to bubble coalescence. The air-in-epoxy resin liquid foam in our work, on the other hand, possessed an initial entrained air volume fraction of ~70%, which is close to the limit of the close-packing of spheres of a given volume (~74%) [56], prior to bubble expansion. As a result, the air bubbles do not have much free space to expand upon heating, leading to the coalescence of the entrapped air bubble, resulting in the formation of pore throats within the foam-templated macroporous polymers.

4.0 Conclusions

In our previous work [29], we showed that high performance bio-based epoxy macroporous polymers can be produced using a simple blowing agent- and stabiliser-free foam-templating method. In this study, we successfully increased the porosity of the foam-templated bio-based macroporous polymers from 71% to as high as 85% by heating the air-in-resin liquid foam prior to its gelation. The heating of this liquid foam decreased the viscosity of the resin

surrounding the air bubbles and increased the pressure inside the air bubbles, leading to the isotropic expansion of air bubbles trapped within the liquid foam. It was also observed that the increase in porosity of the macroporous polymers was also accompanied by an increase in average pore diameter and pore throat frequency.

The fabricated macroporous polymers also possessed high compression properties. Macroporous polymers with a porosity of 71% possessed compression modulus and strength of 231 MPa and 5.9 MPa, respectively. The compression modulus and strength of macroporous polymers decreased to 58 MPa and 1.9 MPa, respectively, when the porosity was increased to 85%. The average molecular weight between crosslinks, compression, tension and flexural properties of the pore wall materials (struts) were found to be similar for all samples. In situ micro-compression SEM tests showed larger pores deformed more compared to smaller pores and the cracks were easy to initiate from the pore throats of the macroporous polymers. Therefore, the decrease in compression properties of the foam-templated macroporous polymers is due to the decrease in foam density and the increase in pore throat frequency.

Supporting information

Videos of the in-situ SEM micro-compression test on the macroporous polymers.

Acknowledgements

The authors would like to thank Imperial College London and China Scholarship Council for funding WS. We also greatly acknowledge funding provided by the UK Engineering and Physical Science Research Council (grant number: EP/M012247/1).

References

1. Polymer Foam Market by Type (PU, PS, PVC, Phenolic, Polyolefin, Melamine, and Other), by Application (Packaging, Building & Construction, Furniture & Bedding, Automotive, and Others), by Region (North America, Europe, Asia-Pacific, and Row) - Global Forecasts to 2021. Markets and Markets Inc., Vancouver, 2016.

2. Eaves D. Handbook of Polymer Foams: Rapra Technology, 2004.
3. Mills N. Polymer Foams Handbook: Engineering and Biomechanics Applications and Design Guide: Elsevier Science, 2007.
4. Landrock AH. Handbook of Plastic Foams: Types, Properties, Manufacture and Applications: Elsevier Science, 1995.
5. Polymeric Foams. BCC-Research, 2015. pp. http://www.bccresearch.com/market-research/plastics/polymeric-foams-report-pls008h.html.
6. Andersen PJ, Kumar A, and Hodson SK. Materials Research Innovations 1999;3(1):2-8.
7. Soykeabkaew N, Supaphol P, and Rujiravanit R. Carbohydrate Polymers 2004;58(1):53-63.
8. Tiefenbacher KF. Journal of Macromolecular Science-Pure and Applied Chemistry 1993;A30(9-10):727-731.
9. Kose GT, Kenar H, Hasirci N, and Hasirci V. Biomaterials 2003;24(11):1949-1958.
10. Kose GT, Korkusuz F, Korkusuz P, and Hasirci V. Tissue Engineering 2004;10(7-8):1234-1250.
11. Corre Y-M, Maazouz A, Duchet J, and Reignier J. Journal of Supercritical Fluids 2011;58(1):177-188.
12. Lee ST, Kareko L, and Jun J. Journal of Cellular Plastics 2008;44(4):293-305.
13. Richards E, Rizvi R, Chow A, and Naguib H. Journal of Polymers and the Environment 2008;16(4):258-266.
14. Tang M, Purcell M, Steele JAM, Lee K-Y, McCullen S, Shakesheff KM, Bismarck A, Stevens MM, Howdle SM, and Williams CK. Macromolecules 2013;46(20):8136-8143.
15. Li Y and Ragauskas AJ. Rsc Advances 2012;2(8):3347-3351.
16. Yang LT, Zhao CS, Dai CL, Fu LY, and Lin SQ. Journal of Polymers and the Environment 2012;20(1):230-236.
17. Dworakowska S, Cornille A, Bogdal D, Boutevin B, and Caillol S. European Journal of Lipid Science and Technology 2015;117(11):1893-1902.
18. Altuna FI, Esposito L, Ruseckaite RA, and Stefani PM. Composites Part A-Applied Science and Manufacturing 2010;41(9):1238-1244.
19. Mondy LA, Rao RR, Moffat H, Adolf D, and Celina M. Structural Epoxy Foams. Epoxy Polymers: Wiley-VCH Verlag GmbH & Co. KGaA, 2010. pp. 303-324.
20. Frisch KC and Saunders JH. Plastic Foams: Marcel Dekker Incorporated, 1972.
21. Shutov FA, Henrici-Olive G, and Olive S. Integral/Structural Polymer Foams: Technology, Properties and Applications: Springer Berlin Heidelberg, 2013.
22. Park SJ, Jin FL, and Lee CJ. Materials Science and Engineering a-Structural Materials Properties Microstructure and Processing 2005;402(1-2):335-340.
23. Zhang L, Roy S, Chen Y, Chua EK, See KY, Hu X, and Liu M. Acs Applied Materials & Interfaces 2014;6(21):18644-18652.
24. Klempner D, Sendijarevi′c V, and Aseeva RM. Handbook of Polymeric Foams and Foam Technology: Hanser Publishers, 2004.
25. Lee JHL. Foamed epoxy resin using trialkoxyboroxines as catalytic blowing agents. U.S. Patent 3,378,504, 1968.
26. Russick EM and Rand PB. Epoxy foams using multiple resins and curing agents. U.S. Patent 6,110,982, 2000.
27. Takiguchi O, Ishikawa D, Sugimoto M, Taniguchi T, and Koyama K. Journal of Applied Polymer Science 2008;110(2):657-662.
28. Wade RC and Letendre C. Journal of Cellular Plastics 1980;16(1):32-35.

29. Lau THM, Wong LLC, Lee K-Y, and Bismarck A. Green Chemistry 2014;16(4):1931-1940.
30. Lee K-Y, Wong LLC, Blaker JJ, Hodgkinson JM, and Bismarck A. Green Chemistry 2011;13(11):3117-3123.
31. Shutov FA. Advances in Polymer Science 1983;51:155-225.
32. Tobolsky AV. Journal of Polymer Science Part C: Polymer Symposia 1965;9(1):157-191.
33. Murayama T and Bell JP. Journal of Polymer Science Part A-2-Polymer Physics 1970;8(3):437-445.
34. Landel RF and Nielsen LE. Mechanical Properties of Polymers and Composites, Second Edition: Taylor & Francis, 1993.
35. Lapique F and Redford K. International Journal of Adhesion and Adhesives 2002;22(4):337-346.
36. Li HM and Zhang BM. Polymer Engineering and Science 2016;56(6):617-621.
37. Simpson JO and Bidstrup SA. Journal of Polymer Science Part B-Polymer Physics 1995;33(1):55-62.
38. Ikem VO, Menner A, Horozov TS, and Bismarck A. Advanced Materials 2010;22(32):3588-3592.
39. Menner A and Bismarck A. Macromolecular Symposia 2006;242:19-24.
40. The mechanics of foams: basic results. In: Gibson LJ and Ashby MF, editors. Cellular Solids: Structure and Properties. Cambridge: Cambridge University Press, 1997. pp. 175-234.
41. Thornton PH and Magee CL. Metallurgical Transactions a-Physical Metallurgy and Materials Science 1975;6(9):1801-1807.
42. Thornton PH and Magee CL. Metallurgical Transactions A 1975;6(6):1253-1263.
43. Xu ZG, Fu JW, Luo TJ, and Yang YS. Materials & Design 2012;34:40-44.
44. Taherishargh M, Sulong MA, Belova IV, Murch GE, and Fiedler T. Materials & Design 2015;66:294-303.
45. Liu DM. Ceramics International 1997;23(2):135-139.
46. Cordell JM, Vogl ML, and Johnson AJW. Journal of the Mechanical Behavior of Biomedical Materials 2009;2(5):560-570.
47. Li ZY, Yang LL, Li Y, Yang YN, Zhou CH, Ding YB, and Zhao JP. Materials & Design 2013;45:52-55.
48. Arezoo S, Tagarielli VL, Petrinic N, and Reed JM. Journal of Materials Science 2011;46(21):6863-6870.
49. Zenkert D and Burman M. Composites Science and Technology 2009;69(6):785-792.
50. Deshpande VS and Fleck NA. Acta Materialia 2001;49(10):1859-1866.
51. Chen CP and Lakes RS. Cellular Polymers 1995;14(3):186-202.
52. Deshpande VS and Fleck NA. International Journal of Impact Engineering 2000;24(3):277-298.
53. Huang RX and Li PF. Composites Part B-Engineering 2015;78:401-408.
54. Pellegrino A, Tagarielli VL, Gerlach R, and Petrinic N. International Journal of Impact Engineering 2015;75:214-221.
55. Briscoe BJ, Chaudhary BI, and Savvas T. Cellular Polymers 1993;12(3):171-193.
56. Hales TC. Mathematical Intelligencer 1994;16(3):47-58.

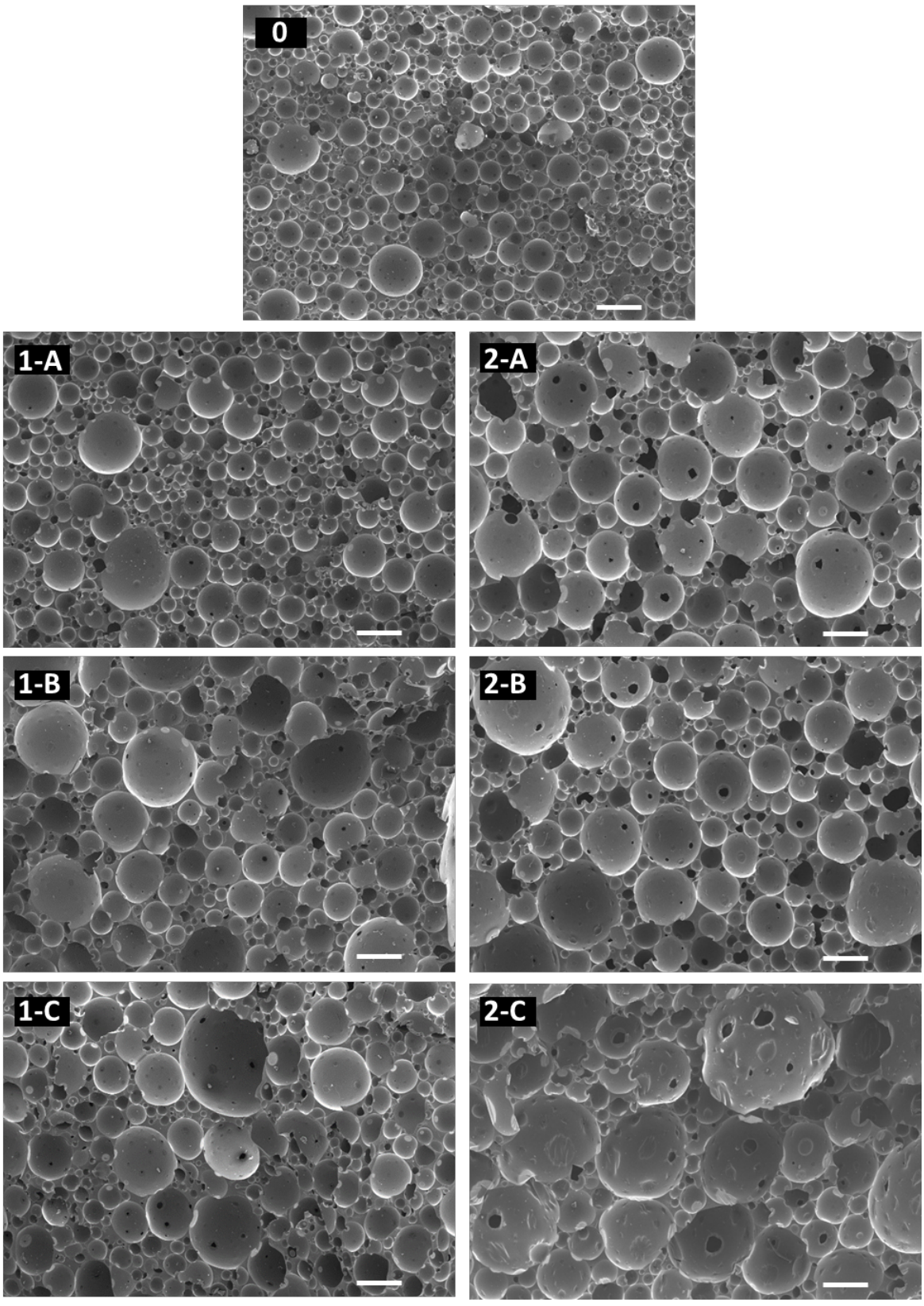

Figure 1. Scanning electron micrographs of the fabricated biobased macroporous polymers. Sample **0**: cure at room temperature for 24 h and post-cure at 40 °C for 24 h. **1** and **2** represent standing time at room temperature of 1 h and 30 min after initial mixing, respectively. **A**, **B** and **C** represent polymerising temperature of 80 °C, 100 °C and 120 °C, respectively. (scale bar = 500 μm).

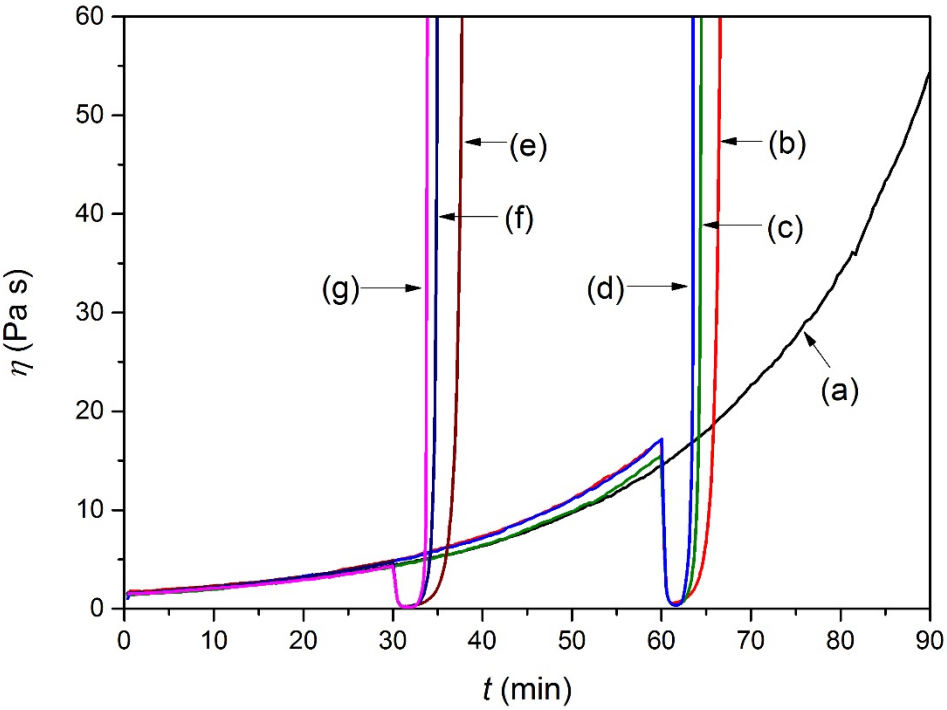

Figure 2. Viscosity of the resin-hardener mixture polymerised at different conditions. (a) cure at room temperature. (b), (c) and (d) cure at room temperature for 1 h and post-cure at 80 °C, 100 °C and 120 °C, respectively. (e), (f) and (g) cure at room temperature for 30 min and post-cure at 80 °C, 100 °C and 120 °C, respectively.

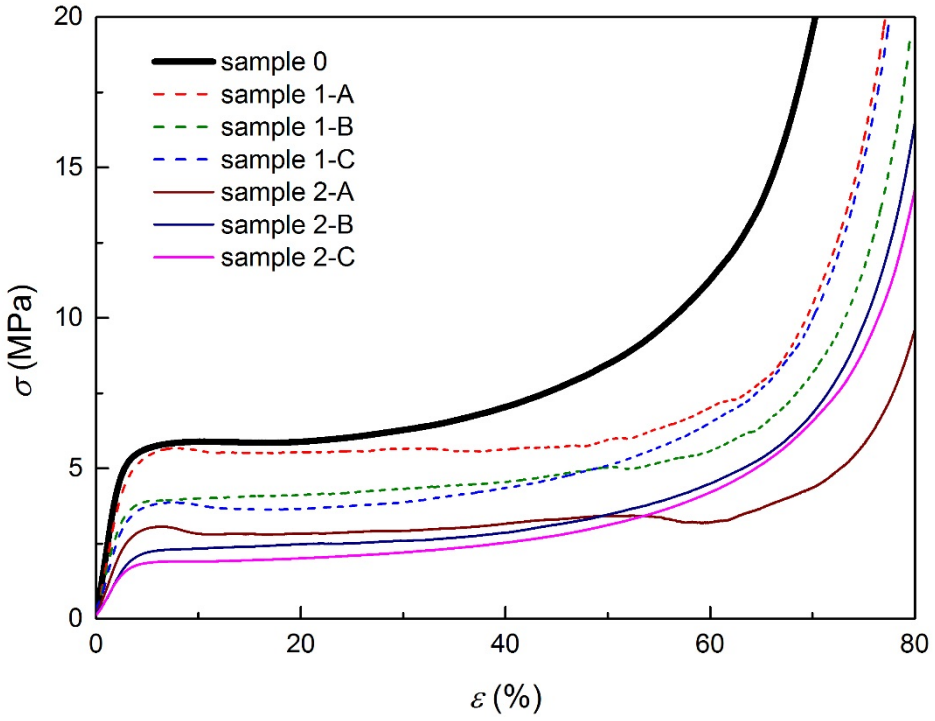

Figure 3. Representative compressive stress-strain curves of the fabricated bio-based macroporous polymers.

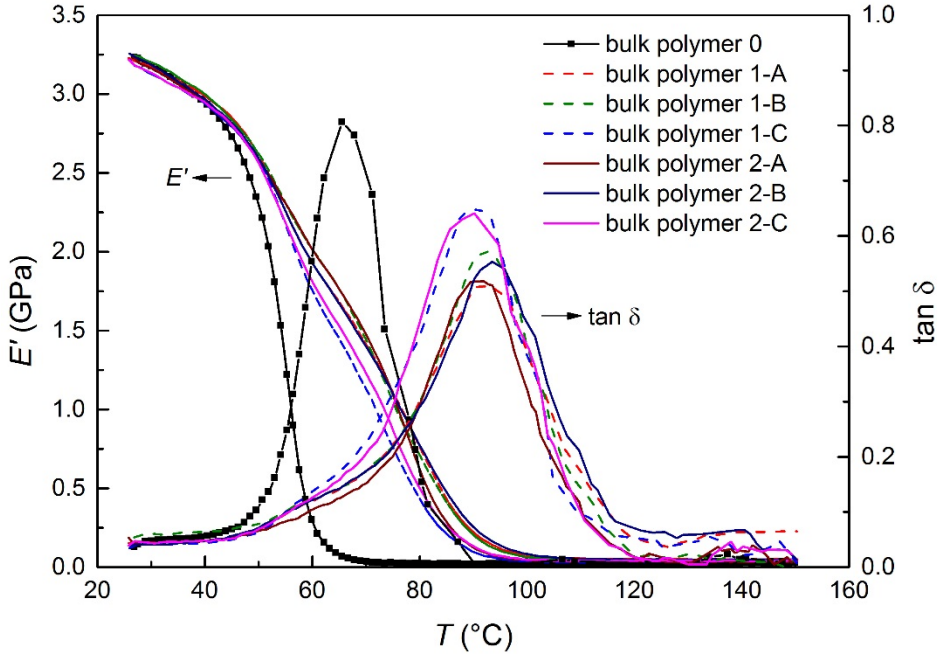

Figure 4. Viscoelastic properties of the bulk polymers polymerised at different conditions.

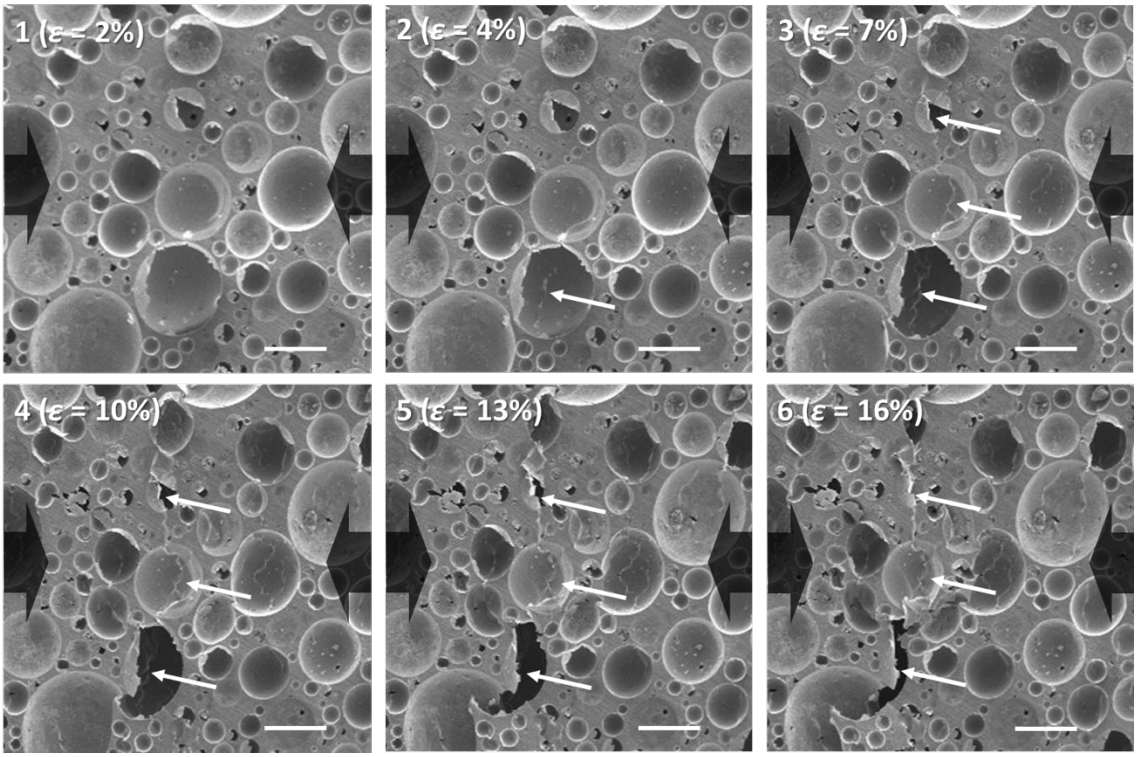

(a)

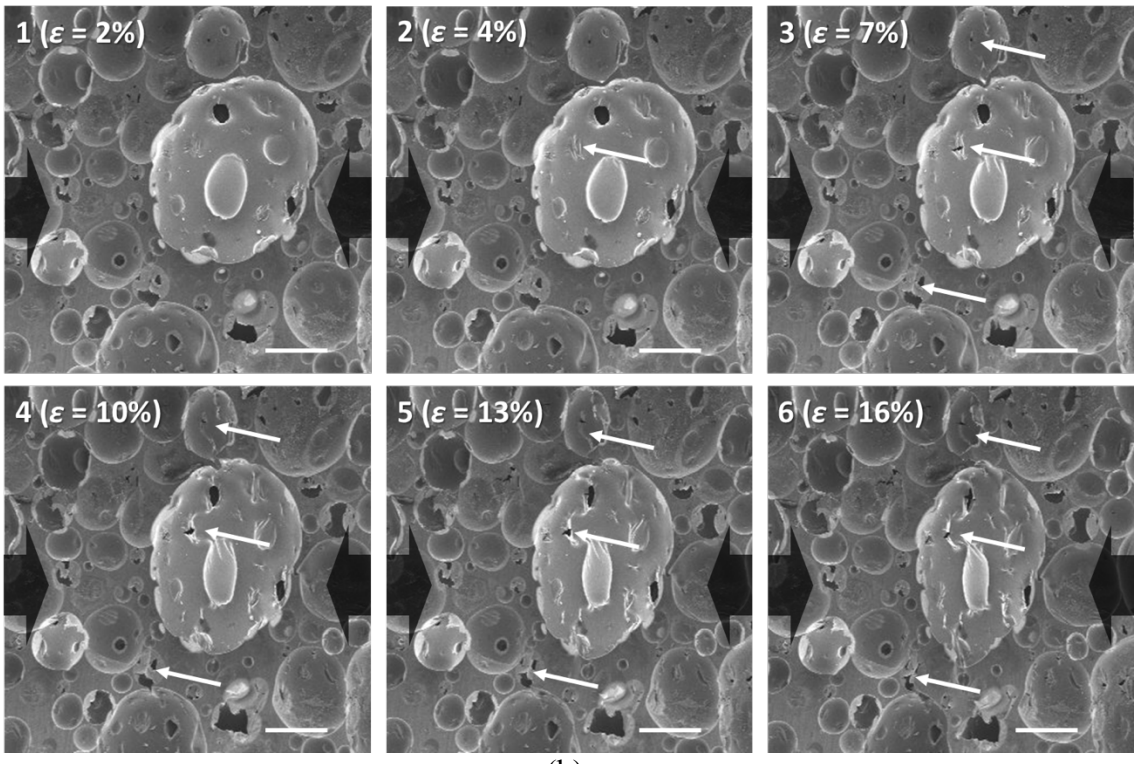

(b)

Figure 5. SEM images of in-situ micro-compression test on sample **0** (a) and sample **2-C** (b) (scale bar = 500 µm).

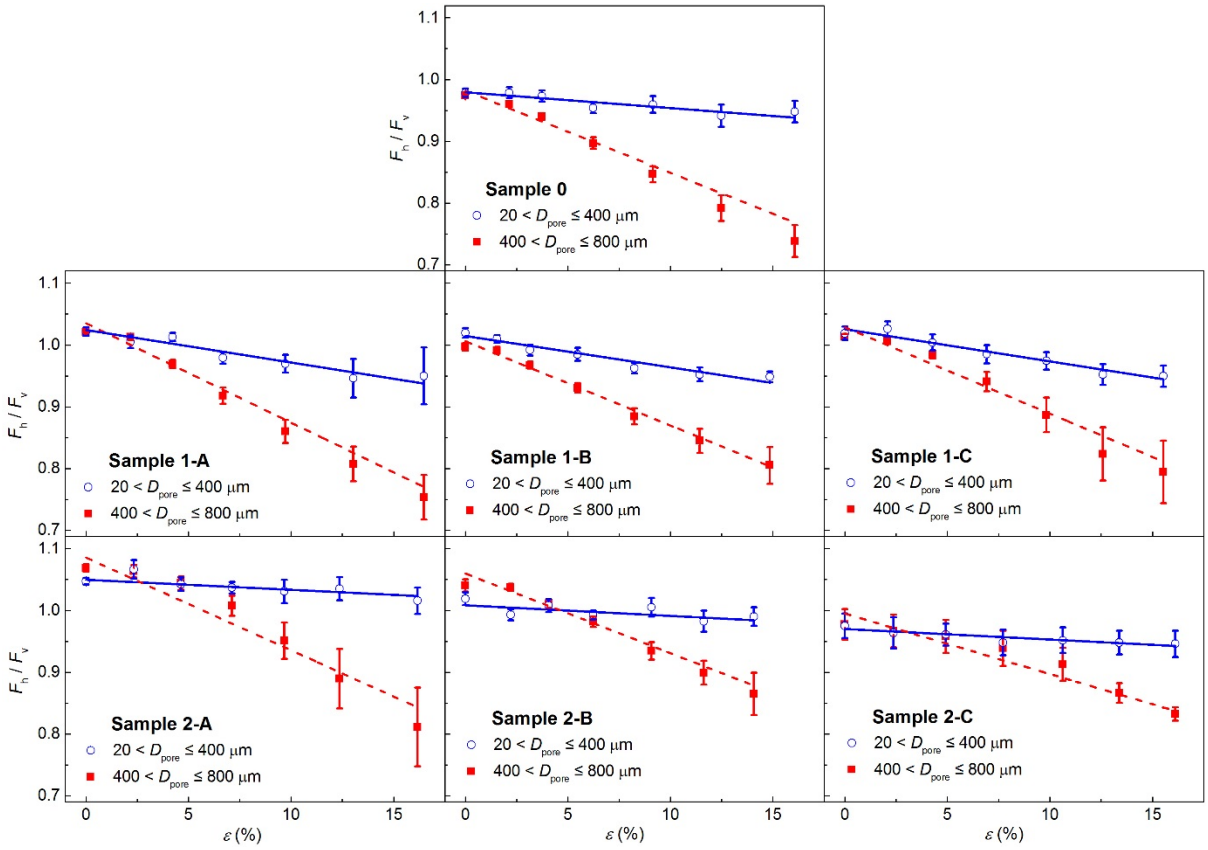

Figure 6. Deformation of pores with different diameter. F_h and F_v denote horizontal and vertical Feret diameter, respectively.

Table 1. Density, porosity and morphological properties of the macroporous polymers. $\rho_f, P, O_V, D_{pore}, T_{wall}, D_{throat}$ and f_{throat} denote density, porosity, open cell content, average pore diameter, mean pore wall thickness, average pore throat diameter and pore throat frequency, respectively

Sample	ρ_f (g/cm^3)	P^a (%)	O_V (%)	D_{pore} (μm)	T_{wall} (μm)	D_{throat} (μm)	f_{throat} (%)
0	0.35 ± 0.02	71 ± 2	2 ± 1	152 ± 114	28 ± 1	18 ± 6	4
1-A	0.31 ± 0.01	74 ± 1	15 ± 1	181 ± 135	30 ± 1	23 ± 9	13
1-B	0.28 ± 0.01	77 ± 1	16 ± 1	187 ± 144	27 ± 1	31 ± 14	17
1-C	0.26 ± 0.02	78 ± 1	24 ± 1	187 ± 143	26 ± 1	36 ± 28	20
2-A	0.21 ± 0.01	82 ± 1	30 ± 1	229 ± 161	25 ± 1	56 ± 34	28
2-B	0.20 ± 0.01	83 ± 1	28 ± 1	248 ± 159	26 ± 1	56 ± 34	24
2-C	0.18 ± 0.01	85 ± 1	29 ± 1	352 ± 277	33 ± 1	89 ± 53	27

[a]Porosity calculated using equation $P = 1 - \frac{\rho_f}{\rho_s}$, and ρ_s is found the same for all samples (1.20 ± 0.01 g/cm^3).

Table 2. Compressive properties of the macroporous polymers. $E_{c,foam}$ and $\sigma_{c,foam}$ denote the compressive modulus and compressive strength of the macroporous polymers, respectively

Sample	$E_{c,foam}$ (MPa)	$\sigma_{c,foam}$ (MPa)
0	231 ± 17	5.9 ± 0.7
1-A	184 ± 10	5.4 ± 0.3
1-B	146 ± 4	4.5 ± 0.1
1-C	125 ± 16	3.8 ± 0.5
2-A	95 ± 3	2.7 ± 0.2
2-B	73 ± 11	2.2 ± 0.3
2-C	58 ± 10	1.9 ± 0.1

Table 3. Viscoelastic properties of the bulk polymers. E', E'_R, T_g and M_c denote the storage modulus at room temperature, the storage modulus of the rubbery plateau evaluated at T_g + 40 K, the mechanical glass transition temperature and the molecular weight between crosslinks, respectively

Sample	E' (GPa)	E'_R (MPa)	T_g (° C)	M_c (g/mol)
0	3.23 ± 0.02	26.9 ± 1.6	65.8 ± 0.2	416 ± 25
1-A	3.08 ± 0.29	44.2 ± 5.9	92.8 ± 0.1	273 ± 37
1-B	3.10 ± 0.20	45.5 ± 5.2	92.3 ± 0.1	264 ± 30
1-C	3.13 ± 0.17	37.1 ± 3.9	89.3 ± 0.9	321 ± 33
2-A	2.92 ± 0.23	43.2 ± 2.1	91.0 ± 0.7	276 ± 13
2-B	2.96 ± 0.48	44.9 ± 5.2	93.1 ± 0.1	268 ± 31
2-C	3.05 ± 0.29	38.0 ± 4.5	91.3 ± 0.9	316 ± 36

Table 4. Mechanical properties of the bulk polymers. $E_C, \sigma_C, E_T, \sigma_T, E_F$ and σ_F denote compressive modulus and strength, tensile modulus and ultimate strength, flexural modulus and ultimate strength, respectively

Sample	E_C (GPa)	σ_C(MPa)	E_T (GPa)	σ_T (MPa)	E_F (GPa)	σ_F (MPa)
0	3.2 ± 0.1	82 ± 1	2.6 ± 0.1	52 ± 1	2.5 ± 0.1	70 ± 2
1-A	3.2 ± 0.2	84 ± 1	2.5 ± 0.1	57 ± 1	2.6 ± 0.1	89 ± 1
1-B	2.9 ± 0.1	81 ± 1	2.5 ± 0.1	55 ± 1	2.5 ± 0.1	80 ± 2
1-C	3.0 ± 0.1	79 ± 1	2.6 ± 0.1	54 ± 1	2.6 ± 0.1	85 ± 2
2-A	3.2 ± 0.2	83 ± 1	2.5 ± 0.1	56 ± 1	2.8 ± 0.1	90 ± 2
2-B	2.9 ± 0.1	80 ± 1	2.5 ± 0.1	55 ± 1	2.5 ± 0.1	72 ± 4
2-C	3.1 ± 0.2	80 ± 1	2.5 ± 0.1	52 ± 1	2.7 ± 0.1	85 ± 2

Table 5. Normalised compressive properties of the fabricated foam-templated macroporous polymers. $E_{\text{c,foam}}, \sigma_{\text{c,foam}}$ and ρ_f denote compressive moduli, strength and foam density of the macroporous polymers, respectively.

Sample	$\frac{E_{\text{c,foam}}}{\rho_f^2}$ (MPa cm^6 g^{-2})	$\frac{\sigma_{\text{c,foam}}}{\rho_f^{1.5}}$ (MPa cm$^{4.5}$ g$^{-1.5}$)
0	1908 ± 133	28.4 ± 0.8
1-A	1951 ± 64	31.8 ± 0.5
1-B	1872 ± 99	30.8 ± 0.6
1-C	1830 ± 363	28.3 ± 1.7
2-A	2139 ± 93	27.7 ± 1.2
2-B	1778 ± 188	24.3 ± 1.9
2-C	1713 ± 259	24.4 ± 0.9